A Universal Surface Fixed Charge Reconstruction Strategy to Minimize Contact Loss of Wide Bandgap Perovskite Photovoltaics

Yaxiong Guo[1,2], Fang Yao[3], Yunchen Zhang[1], Guoyi Chen[2], Shengjie Du[2], Zixi Yu[2], Hai Zhou[4], Weijun Ke[2*], Chun Li[1*], Guojia Fang[2,3*]*

[1] School of Optoelectronic Science and Engineering, University of Electronic Science and Technology of China, Chengdu 610054, P. R. China

[2] Key Lab of Artifcial Micro- and Nano-Structures of Ministry of Education of China, School of Physics and Technology, Wuhan University, Wuhan 430072, P. R. China

[3] School of Electronics and Electrical Engineering, Wuhan Textile University, Wuhan 430200, P. R. China

[4] International School of Microelectronics, Dongguan University of Technology, Dongguan 523808, P. R. China

E-mail: gjfang@whu.edu.cn; lichun@uestc.edu.cn; weijun.ke@whu.edu.cn; hizhou@dgut.edu.cn;

Materials and Methods

Materials

[4-(3,6-Dimethyl-9H-carbazol-9-yl)butyl]phosphonic Acid (Me-4PACz), Lead iodide (PbI_2, 99.9%), lead bromide ($PbBr_2$, 99.9%) were purchased from TCI. Formamidinium iodide (FAI, 99.9%) and cesium iodide (CsI, 99.9%) were purchased from Alfa Aesar. C60 (99.9%), bathocuproine (BCP, 99.9%) were purchased from Xi'an Polymer Light Technology. All other solvents were purchased from Sigma-Aldrich. To form methylammonium-free wide-bandgap perovskite precursor solutions, CsI, FAI, PbI_2 and $PbBr_2$ were prepared in the way corresponding to the exact stoichiometry for the hybrid perovskite composition[i.e. $Cs_xFA_{1-x}Pb(I_{1-y}Br_y)_3$; (i) for 1.65 eV cells, x = 0.20 and y = 0.20, abbreviated as $Cs_{20}Br_{20}$; (ii) for 1.79 eV cells, x = 0.20 and y = 0.45, abbreviated as $Cs_{20}Br_{45}$; (iii) for 1.91 eV cells, x = 0.15 and y = 0.65, abbreviated as $Cs_{15}Br_{65}$] in a mixed organic solvent system of N, N-dimethylformamide (DMF): dimethyl sulfoxide (DMSO) at the volume ratio (4:1).

Film deposition, surface passivation, and solar cell fabrication

Indium tin oxide (ITO) coated glass substrates were cleaned in a series of ultrasonic cleaning baths using deionized water, acetone and isopropanol in the sequence. Immediately, substrates were dried with compressed nitrogen and then treated with UV-Ozone for 15 minutes before use. After cleaning procedure, Me-4PACz (0.5 mg mL^{-1} in ethanol) was deposited onto the substrate at 3,000 rpm for 30 s, followed by thermal annealing at 100°C for 10 min. The perovskite precursor was deposited in a nitrogen-filled glovebox, starting at 1,000 rpm for 5 s then 5,000 rpm for 30 s. Before the end of the spinning process, a solvent-quenching method was used by dropping ether of 300 μL onto the spinning substrates. The thermal annealing process was then carried out at 100°C for 10 minutes for the formation of the perovskite layer.

For the PT/$PDAI_2$ devices, 6 mM PT was dissolved in isopropanol solvent. Then, 100 μL mixed solution was filtered and dynamically spin-coated on the perovskite films at 4500 rpm for 20 s, followed by annealing at 100°C for 5 min. The solar cells were completed by thermal evaporation of C_{60} (20 nm) and BCP (7 nm) and Cu electrodes (100 nm) under high vacuum (5×10^{-4} Pa) using a thermal evaporator placed in nitrogen-filled glovebox.

Characterizations

Current-density-voltage (*J-V*) characteristics. The J-V characteristics were measured in a nitrogen glovebox at room temperature using a Keithley 2401 digital source-meter under simulated AM 1.5 G irradiation from a Xe arc lamp (Sciencetech A1 Light Line Class AAA solar simulator). The light intensity was calibrated by a Sciencetech SCI-REF-Q silicon cell from before measurement, and no preconditioning was applied. The scanning step was 20 mV with a scanning rate of 70 mV/s. The active area of the solar cells was defined by an opaque metal mask with an aperture area of 0.07 cm^2.

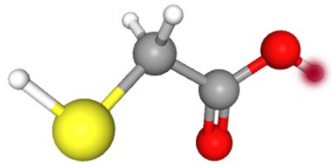

Fig. S1. Molecule of Potassium Thioglycolate (PT). (White: hydrogen, grey: carbon, red: oxygen, yellow: sulfur, dark red: potassium)

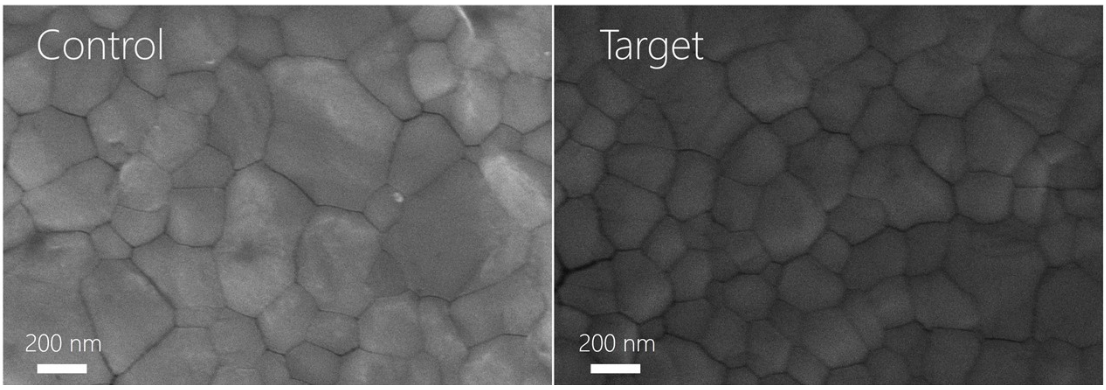

Fig. S2. SEM top-view images taken from control and $PT/PDAI_2$-treated films.

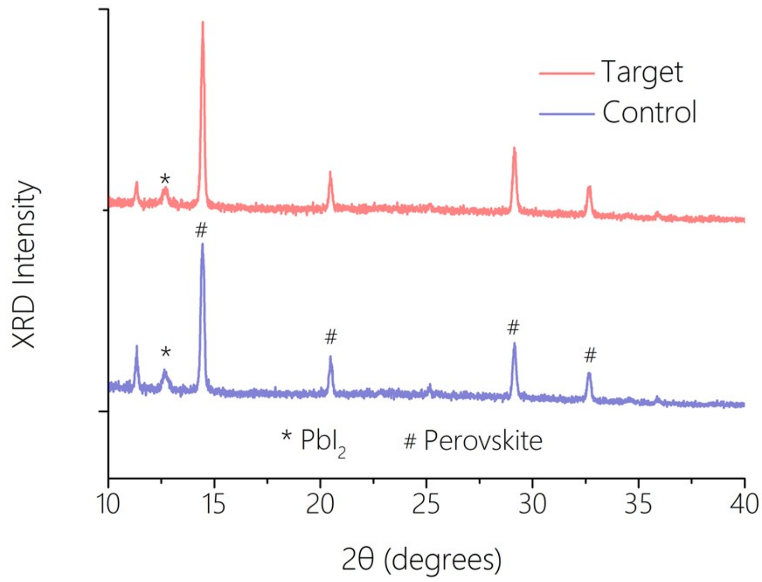

Fig. S3. XRD patterns of perovskite thin films for control and treated with $PT/PDAI_2$.

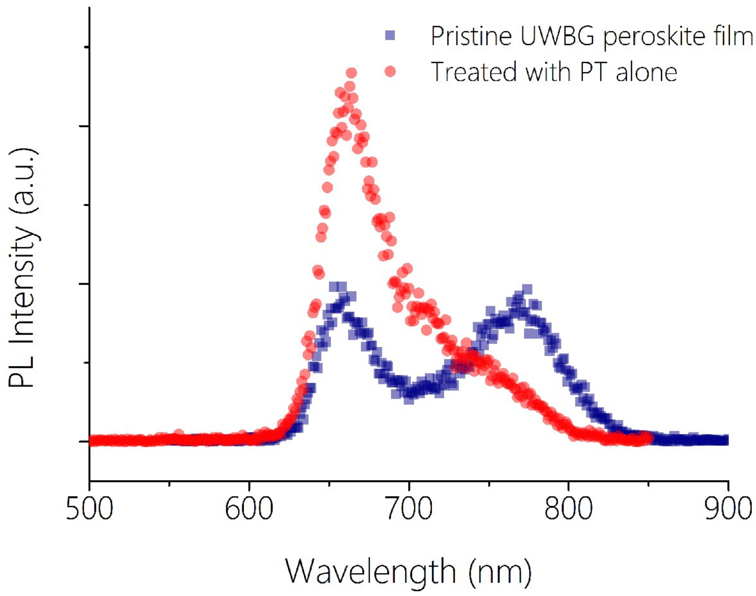

Fig. S4. PL spectra of the pristine and PT-modified perovskite films from top surface.

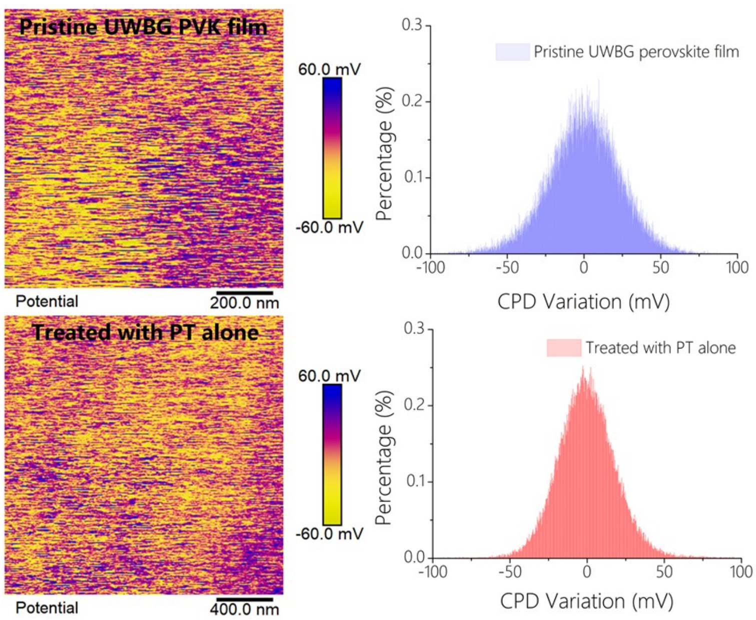

Fig. S5. KPFM map and corresponding statistical distribution of surface potential for pristine and PT-modified perovskite films from top surface.

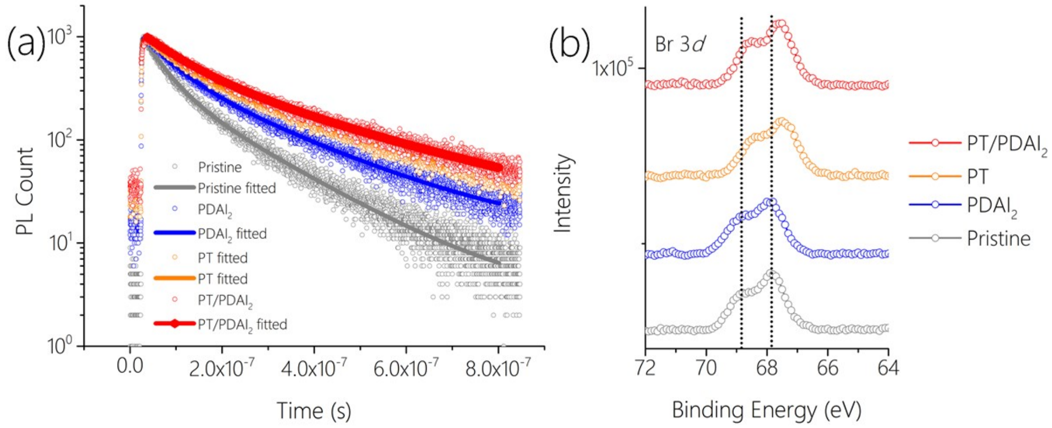

Fig. S6. (a) TRPL spectra of perovskite films with different treatments. (b) Br 3d XPS spectra of perovskite surface with different treatments.

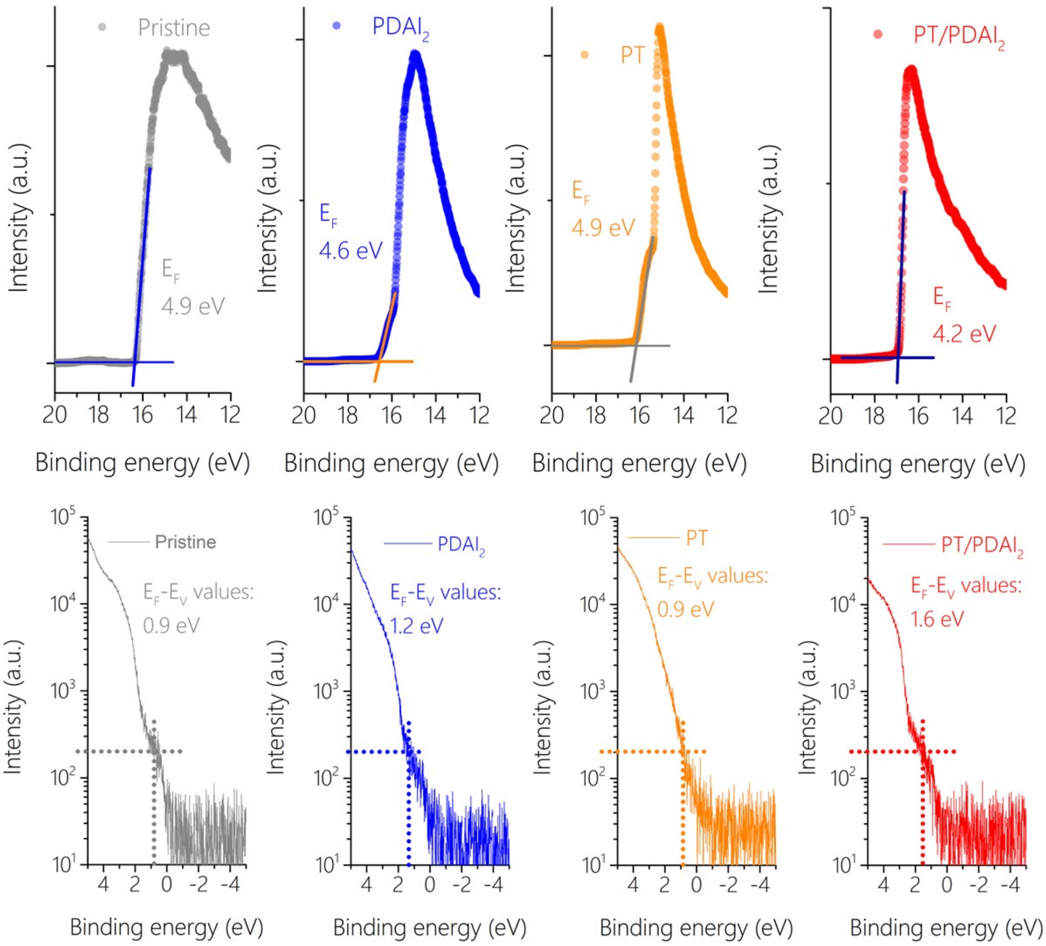

Fig. S7. UPS spectra of perovskite films with different treatments.

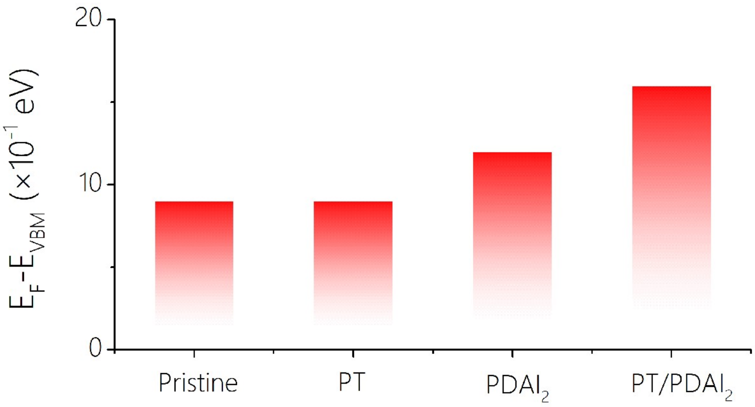

Fig. S8. A comparison of differences in the energy level between the valence band maximum and Fermi level for perovskite surface with different treatments obtained from UPS results.

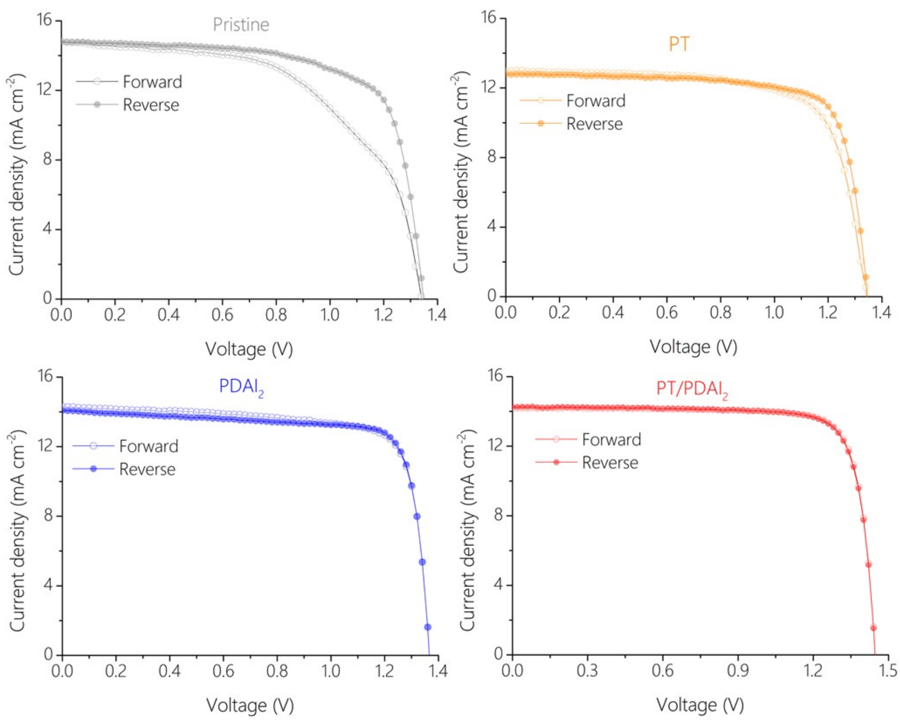

Fig. S9. *J-V* characteristic of the UWBG PSC based on different surface treatments.

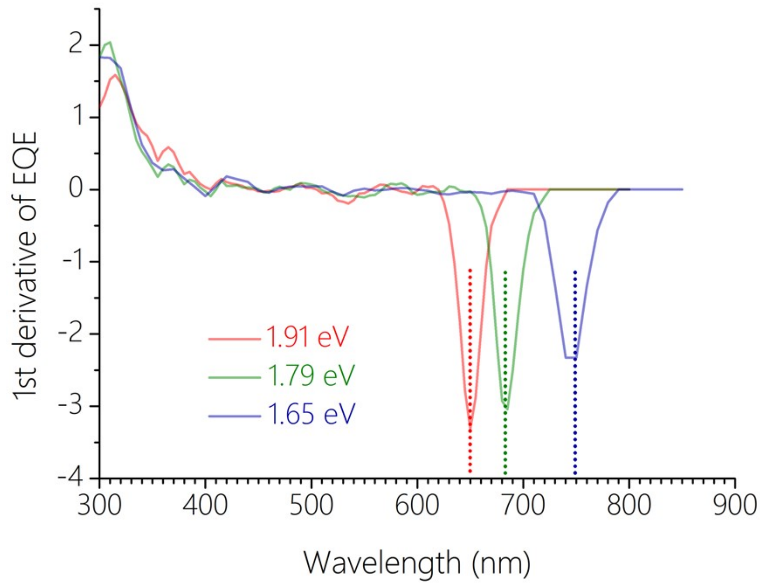

Fig. S10. Photovoltaic bandgap values determined by inflection points of EQE curves.

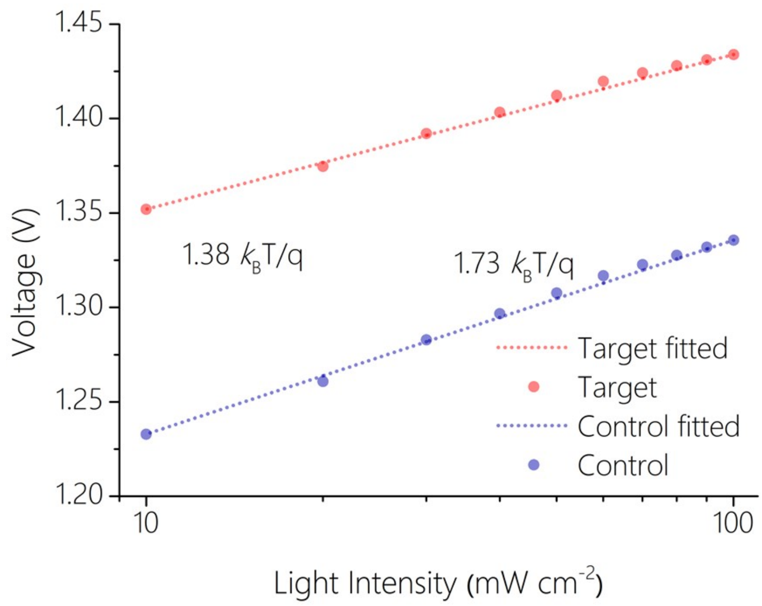

Fig. S11. Light-intensity dependence of V_{OC} measurement related to pristine and Cs15Br65 devices.

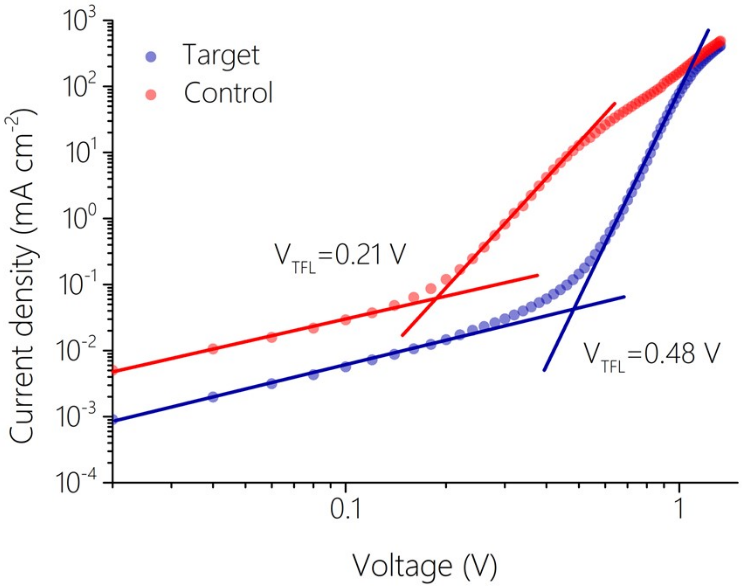

Fig. S12. SCLC analysis for hole-only devices for control and PT/$PDAI_2$-treated devices.

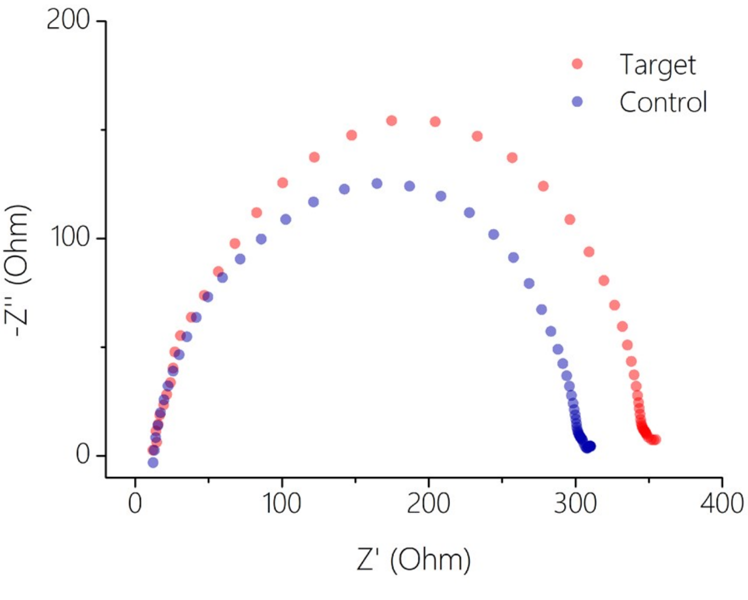

Fig. S13. Electrochemical impedance spectroscopy (EIS) plots for control and PT/$PDAI_2$-treated devices.

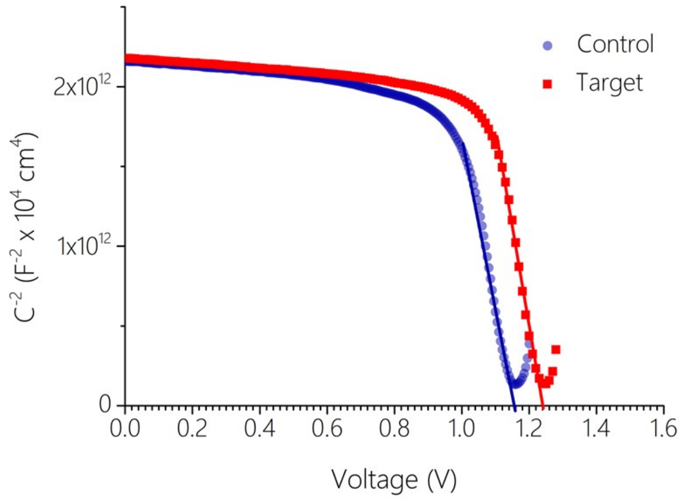

Fig. S14. Mott-Schottky curves of *C*-*V* measurement for control and target devices.

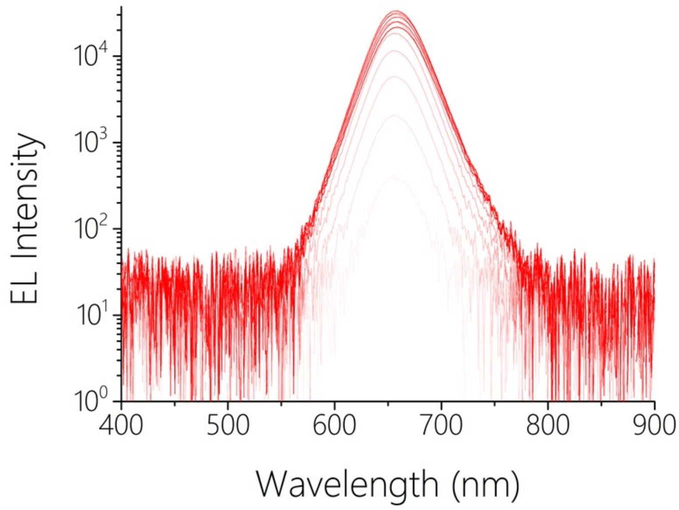

Fig. S15. Electroluminescence (EL) spectra of the $Cs_{15}Br_{65}$ PSCs under the different bias.

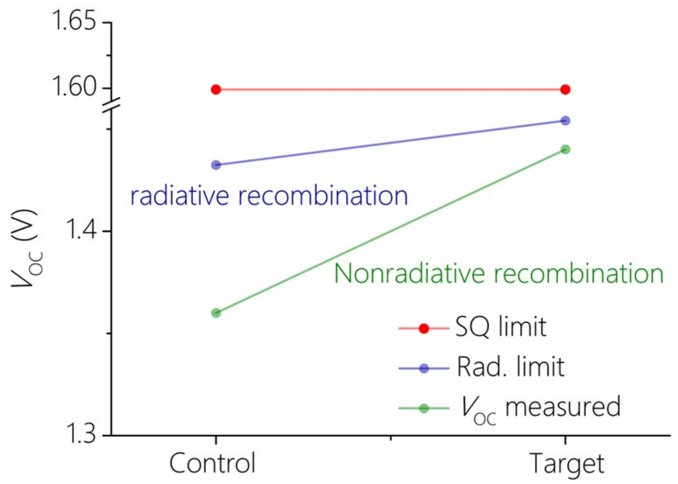

Fig. S16. Detailed analysis of V_{OC} loss for target and control devices.

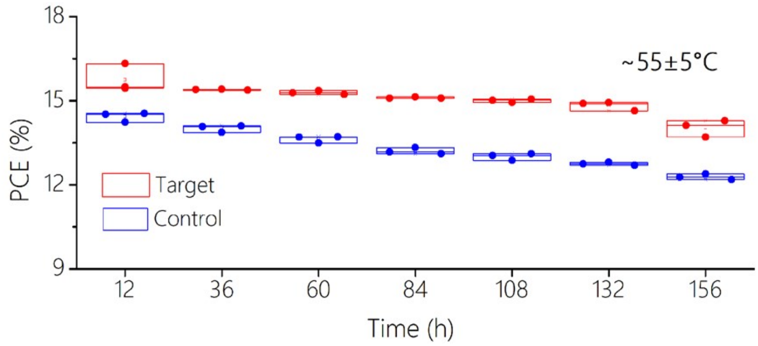

Fig. S17. PCE of unencapsulated devices as a function of measurement time under ~55°C in N_2.

Table S1. Summary of carrier lifetimes. PL lifetimes based on a biexponential fitting of curves.

Treatment	τ_1	τ_2	$\langle\tau\rangle$
Pristine	45.4 ns	167.0 ns	90.3 ns
PT	70.2 ns	259.8 ns	172.3 ns
$PDAI_2$	61.0 ns	216.3 ns	133.7 ns
PT/$PDAI_2$	89.6 ns	309.1 ns	195.2 ns
$PDAI_2$/C_{60} (C_{60} side)	3.2 ns	38.6 ns	16.1 ns
PT/$PDAI_2$ /C_{60} (C_{60} side)	37.3 ns	115.7 ns	60.4 ns

Table S2. Device performance of the UWBG PSCs.

Treatment		V_{OC} (V)	J_{SC} (mA cm^{-2})	FF (%)	PCE (%)
Pristine	Forward	1.3396	14.83511	56.0607	11.14098
	Reverse	1.34761	14.77048	70.34792	14.00266
PT	Forward	1.33917	13.01678	71.82067	12.51953
	Reverse	1.34478	12.79329	76.84819	13.22105
$PDAI_2$	Forward	1.36418	14.30756	77.73369	15.29419
	Reverse	1.36418	14.06975	79.77507	15.44645
PT/$PDAI_2$	Forward	1.4443	14.11118	81.81786	16.67517
	Reverse	1.44382	14.38088	81.25213	16.87068

Table S3. Corresponding PV performance parameters obtained for PT/$PDAI_2$-treated solar cells shown in Fig. 4 using $Cs_{15}Br_{65}$ (i.e., 1.91 eV) as the light absorbers.

$Cs_{15}Br_{65}$	V_{OC} (V)	J_{SC} (mA cm^{-2})	FF (%)	PCE (%)
FB-SC	1.4443	14.11118	81.81786	16.67517
SC-FB	1.44382	14.38088	81.25213	16.87068
FB-SC	1.36418	14.30756	77.73369	15.29419
SC-FB	1.36418	14.06975	79.77507	15.44645

Table S4. Corresponding PV performance parameters obtained for PT/$PDAI_2$-treated solar cells shown in Fig. 4 using $Cs_{20}Br_{45}$ (i.e., 1.79 eV) as the light absorbers.

$Cs_{20}Br_{45}$	V_{OC} (V)	J_{SC} (mA cm^{-2})	FF (%)	PCE (%)
FB-SC	1.36908	17.17021	81.343	19.21026
SC-FB	1.37716	17.14027	82.7096	19.60961
FB-SC	1.31099	17.15411	80.3105	18.06094
SC-FB	1.32526	17.09719	82.03297	18.58721

Table S5. Corresponding PV performance parameters obtained for PT/$PDAI_2$-treated solar cells shown in Fig. 4 using $Cs_{20}Br_{20}$ (i.e., 1.65 eV) as the light absorbers.

$Cs_{20}Br_{20}$	V_{OC} (V)	J_{SC} (mA cm^{-2})	FF (%)	PCE (%)
FB-SC	1.23654	21.4521	83.19177	22.03904
SC-FB	1.24241	21.45792	84.72108	22.53371
FB-SC	1.21297	21.2308	82.62292	21.2751
SC-FB	1.22017	21.23282	84.08526	21.75852

Table S6. Summary of representative reports on performance of 1.63-2.00 eV wide-bandgap inverted PSCs.

E_g/ eV	V_{OC}/ V	J_{SC}/mA cm^{-2}	FF/ %	PCE/ %	Reference	
1.63	1.24	22.9	77.8	22.1	*Advanced Materials* **2022**, *34* (6), 2106280.	1
1.65	1.127	21.69	82	20.04	*ACS Energy Letters* **2021**, 6 (8), 2735-2741.	2
1.65	1.23	21.2	83.8	21.9	*Nature Photonics* **2022**, *16* (8), 588-594.	3
1.65	1.221	21.5	83.3	21.9	*Advanced Energy Materials* **2023**, *13* (2), 2203230.	4
1.65	1.25	21.93	79.48	21.80	*Joule* **2023**, *7* (6), 1363-1381.	5
1.65	**1.242**	**21.45**	**84.72**	**22.53**	**This Work**	
1.66	1.26	21.60	81.60	22.19	*Nano Letters* **2023**, *23* (14), 6705-6712.	6
1.66	1.23	20.74	84.33	21.47	*Advanced Functional Materials* **2023**, *33* (30), 2300860.	7
1.66	1.27	21.14	83.13	22.40	*Advanced Materials* **2024**, *36* (1), 2307987.	8
1.67	1.195	21.11	81.88	20.64	*ACS Nano* **2022**, *16* (7), 10798-10810.	9
1.67	1.19	22.33	81.69	19.76	*Advanced Materials* **2022**, *34* (27), 2201451.	10
1.67	1.262	20.9	82.7	21.8	*Advanced Materials 2024, 36 (9), 2307701.*	11
1.67	1.21	22.40	82.30	22.31	*Advanced Functional Materials* **2023**, *33* (11), 2214381.	12
1.67	1.26	19.6	84.0	20.6	*Science* **2024**, *384* (6697), 767-775.	13
1.67	1.272	21.09	82.01	22.00	*Advanced Energy Materials* **2024**, *14* (7), 2302983.	14
1.68	1.239	21.16	82.50	21.63	*Angewandte Chemie International Edition* **2023**, *62* (11), e202216668.	15
1.68	1.25	21.5	84.5	22.7	*Science* **2023**, *382* (6668), 284-289.	16
1.69	1.21	20.30	82.1	20.18	*Joule* **2022**, *6* (10), 2390-2405.	17

1.69	1.25	20.7	84.2	21.7	*Advanced Materials* ***2024****, 36 (9), 2307701.*	[11]
1.71	1.20	20.81	85.4	21.31	*Advanced Materials* **2023,** *35* (28), 2301879.	[18]
1.72	1.29	18.0	84.8	19.7	*Advanced Materials* ***2024****, 36 (9), 2307701.*	[11]
1.73	1.26	18.44	77.82	18.08	*Nature Photonics* **2021,** *15* (9), 681-689.	[19]
1.73	1.312	18.89	81.6	20.22	*Energy & Environmental Science* **2023,** *16* (5), 2080-2089.	[20]
1.75	1.33	18.7	82.2	20.3	*Science* **2022,** *378* (6626), 1295-1300.	[21]
1.77	1.113	15.4	82.4	14.1	*Joule* **2020,** *4* (7), 1594-1606.	[22]
1.77	1.31	17.80	79.18	18.46	*Nature* **2023,** *618* (7963), 80-86.	[23]
1.77	1.339	16.65	84.65	18.88	*Energy & Environmental Science* **2024,** *17* (1), 202-209.	[24]
1.78	1.35	17.65	83.11	19.83	*Energy & Environmental Science* **2023,** *16* (12), 5992-6002.	[25]
1.79	1.25	16.9	83.0	17.6	*Advanced Materials* **2022,** *34* (11), 2108829.	[26]
1.79	1.26	17.90	78.9	17.80	*Nature Energy* **2022,** *7* (3), 229-237.	[27]
1.79	1.33	17.3	83.9	19.3	*Nature* **2023,** *613* (7945), 676-681.	[28]
1.79	1.35	17.39	83.07	19.5	*Energy & Environmental Science* **2024**, *17* (24), 9580-9589.	[29]
1.79	**1.37**	**17.14**	**82.70**	**19.60**	**This work**	
1.8	1.263	17.4	79.7	17.7	*Advanced Materials* **2022,** *34* (26), 2110356.	[30]
1.8	1.34	18.2	83.9	20.3	*Advanced Materials* **2024,** *36* (6), 2307743.	[31]
1.81	1.35	17.5	82.7	19.6	*Nature Energy* **2024,** *9* (4), 411-421.	[32]
1.85	1.34	15.60	81.00	16.80	*Nature* **2022,** *604* (7905), 280-286.	[33]
1.85	1.360	16.21	83.21	18.14	*Advanced Materials* **2024,** *36* (17), 2306568.	[34]
1.85	1.350	16.78	83.29	18.87	*Advanced Materials* **2023,**	[35]

					35 (49), 2305946.	
1.86	1.280	14.00	78.20	14.00	*Nature Communications* **2019,** *10* (1), 4686.	36
1.86	1.420	14.39	82.00	16.72	*Advanced Functional Materials* **2022,** *32* (43), 2207554.	37
1.86	1.223	16.35	79.62	15.92	*Nano-Micro Letters* **2020,** *12* (1), 170.	38
1.86	1.366	16.10	84.20	18.52	*Joule* **2024,** *8* (9), 2554-2569.	39
1.87	1.260	17.16	80.14	17.37	*Science Bulletin* **2019,** *64* (23), 1743-1746.	40
1.87	1.210	13.42	81.36	13.16	*Advanced Energy Materials* **2020,** *10* (6), 1903085.	41
1.87	1.27	14.2	76	13.7	*Journal of Materials Chemistry A* **2023,** *11* (19), 10254-10266.	42
1.88	1.180	15.80	72.70	13.60	*Advanced Energy Materials* **2019,** *9* (25), 1900896.	43
1.88	1.310	15.81	82.88	17.16	*Advanced Functional Materials* **2023,** *33* (8), 2212599.	44
1.88	1.36	16.1	83.8	18.4	*Nature* **2024,** *635* (8040), 860-866.	45
1.89	1.150	16.82	75.73	14.69	*Joule* **2019,** *3* (10), 2485-2502.	46
1.89	1.280	15.00	77.00	14.80	*ACS Applied Materials & Interfaces* **2019,** *11* (46), 43303-43311.	47
1.91	**1.44**	**14.38**	**81.2**	**16.87**	**This work**	
1.92	1.27	14.8	78.1	14.7	*Advanced Science* **2022,** *9* (28), 2200445.	48
1.92	1.39	14.3	83.5	16.2	*Advanced Materials* **2024,** *36* (49), 2410692.	49
1.92	1.35	15.1	83.7	17	*Advanced Energy Materials* **2023,** *13* (16), 2204347.	50
1.97	1.44	12.8	83	15.3	*Nature Energy* **2024,** *9* (1), 70-80.	51
2.00	1.31	13.5	75.9	13.4	*Nature* **2023,** *618* (7963), 74-79.	52

Table S7. Efficiency parameters of unencapsulated devices as a function of measurement time under~55°C in N_2.

Target/Time (h)	V_{OC} (V)	PCE (%)	FF (%)	J_{SC} (mA/cm^2)	Control/Time (h)	V_{OC} (V)	PCE (%)	FF (%)	J_{SC} (mA/cm^2)
Sample1/12	1.43015	16.34074	81.92694	13.94641	Sample412	1.39607	14.5406	74.16718	14.04314
Sample2/12	1.40183	15.50678	79.82269	13.85798	Sample5/12	1.40118	14.50809	76.77603	13.48625
Sample3/12	1.4105	15.45611	81.24302	13.48783	Sample6/12	1.39471	14.22525	77.66716	13.1322
Sample1/36	1.40693	15.42206	80.49062	13.61832	Sample4/36	1.36535	14.09469	75.83913	13.6119
Sample2/36	1.39394	15.41546	80.70947	13.70209	Sample5/36	1.37499	14.06851	73.87376	13.85028
Sample3/36	1.40046	15.39058	81.25783	13.52446	Sample6/36	1.3872	13.86073	70.64615	14.14359
Sample1/60	1.41712	15.37466	80.56643	13.46618	Sample4/60	1.38178	13.70076	75.01674	13.21745
Sample2/60	1.39025	15.30399	81.43427	13.5177	Sample5/60	1.37915	13.69181	74.76406	13.27872
Sample3/60	1.40679	15.23311	79.97714	13.53919	Sample6/60	1.37506	13.48239	74.67055	13.13095
Sample1/84	1.41023	15.15669	78.77639	13.64325	Sample4/84	1.35926	13.3194	71.94906	13.61936
Sample2/84	1.3965	15.10377	79.6725	13.57485	Sample5/84	1.38228	13.16665	67.25276	14.16341
Sample3/84	1.39098	15.09873	78.80291	13.77453	Sample6/84	1.37602	13.09798	71.99076	13.22214
Sample1/108	1.41508	15.06537	80.75158	13.184	Sample4/108	1.38226	13.09652	71.23416	13.30079
Sample2/108	1.40782	15.0313	77.50971	13.77502	Sample5/108	1.37921	13.04209	75.11616	12.58881
Sample3/108	1.41469	14.95105	80.72073	13.09259	Sample6/108	1.37255	12.85968	70.23663	13.33946
Sample1/132	1.39499	14.94899	80.59223	13.29679	Sample4/132	1.36689	12.79586	68.70295	13.62577
Sample2/132	1.41323	14.91036	80.04152	13.18133	Sample5/132	1.35785	12.74176	73.45903	12.7742
Sample3/132	1.37272	14.64928	81.56212	13.08415	Sample6/132	1.3763	12.68897	71.95711	12.81271
Sample1/156	1.40654	14.30395	78.29524	12.98877	Sample4/156	1.36837	12.38105	69.23223	13.06912
Sample2/156	1.37485	14.13692	77.45033	13.27632	Sample5/156	1.37372	12.26953	72.01712	12.40205
Sample3/156	1.33612	13.71925	80.36396	12.77684	Sample6/156	1.36178	12.17763	67.93375	13.16349

Reference

1. Li, Y.; Xu, W.; Mussakhanuly, N.; Cho, Y.; Bing, J.; Zheng, J.; Tang, S.; Liu, Y.; Shi, G.; Liu, Z.; Zhang, Q.; Durrant, J. R.; Ma, W.; Ho-Baillie, A. W. Y.; Huang, S., Homologous Bromides Treatment for Improving the Open-Circuit Voltage of Perovskite Solar Cells. *Advanced Materials* **2022,** *34* (6), 2106280.
2. Wang, X.; Chen, Y.; Zhang, T.; Wang, X.; Wang, Y.; Kan, M.; Miao, Y.; Chen, H.; Liu, X.; Wang, X.; Shi, J.; Zhang, L.; Zhao, Y., Stable Cesium-Rich Formamidinium/Cesium Pure-Iodide Perovskites for Efficient Photovoltaics. *ACS Energy Letters* **2021,** *6* (8), 2735-2741.
3. Yang, G.; Ni, Z.; Yu, Z. J.; Larson, B. W.; Yu, Z.; Chen, B.; Alasfour, A.; Xiao, X.; Luther, J. M.; Holman, Z. C.; Huang, J., Defect engineering in wide-bandgap perovskites for efficient perovskite–silicon tandem solar cells. *Nature Photonics* **2022,** *16* (8), 588-594.
4. Liu, Z.; Zhu, C.; Luo, H.; Kong, W.; Luo, X.; Wu, J.; Ding, C.; Chen, Y.; Wang, Y.; Wen, J.; Gao, Y.; Tan, H., Grain Regrowth and Bifacial Passivation for High-Efficiency Wide-Bandgap Perovskite Solar Cells. *Advanced Energy Materials* **2023,** *13* (2), 2203230.
5. Li, Z.; Li, X.; Chen, X.; Cui, X.; Guo, C.; Feng, X.; Ren, D.; Mo, Y.; Yang, M.; Huang, H.; Jia, R.; Liu, X.; Han, L.; Dai, S.; Cai, M., In situ epitaxial growth of blocking structure in mixed-halide wide-band-gap perovskites for efficient photovoltaics. *Joule* **2023,** *7* (6), 1363-1381.

6. Song, Z.; Yang, J.; Dong, X.; Wang, R.; Dong, Y.; Liu, D.; Liu, Y., Inverted Wide-Bandgap 2D/3D Perovskite Solar Cells with >22% Efficiency and Low Voltage Loss. *Nano Letters* **2023,** *23* (14), 6705-6712.
7. Guan, H.; Zhang, W.; Liang, J.; Wang, C.; Hu, X.; Pu, D.; Huang, L.; Ge, Y.; Cui, H.; Zou, Y.; Fang, G.; Ke, W., Low-Dimensional 2-thiopheneethylammonium Lead Halide Capping Layer Enables Efficient Single-Junction Methylamine-Free Wide-Bandgap and Tandem Perovskite Solar Cells. *Advanced Functional Materials* **2023,** *33* (30), 2300860.
8. Guan, H.; Zhou, S.; Fu, S.; Pu, D.; Chen, X.; Ge, Y.; Wang, S.; Wang, C.; Cui, H.; Liang, J.; Hu, X.; Meng, W.; Fang, G.; Ke, W., Regulating Crystal Orientation via Ligand Anchoring Enables Efficient Wide-Bandgap Perovskite Solar Cells and Tandems. *Advanced Materials* **2024,** *36* (1), 2307987.
9. Tao, J.; Liu, X.; Shen, J.; Han, S.; Guan, L.; Fu, G.; Kuang, D.-B.; Yang, S., F-Type Pseudo-Halide Anions for High-Efficiency and Stable Wide-Band-Gap Inverted Perovskite Solar Cells with Fill Factor Exceeding 84%. *ACS Nano* **2022,** *16* (7), 10798-10810.
10. Li, R.; Chen, B.; Ren, N.; Wang, P.; Shi, B.; Xu, Q.; Zhao, H.; Han, W.; Zhu, Z.; Liu, J.; Huang, Q.; Zhang, D.; Zhao, Y.; Zhang, X., CsPbCl3-Cluster-Widened Bandgap and Inhibited Phase Segregation in a Wide-Bandgap Perovskite and its Application to NiO-Based Perovskite/Silicon Tandem Solar Cells. *Advanced Materials* **2022,** *34* (27), 2201451.
11. Li, S.; Zheng, Z.; Ju, J.; Cheng, S.; Chen, F.; Xue, Z.; Ma, L.; Wang, Z., A Generic Strategy to Stabilize Wide Bandgap Perovskites for Efficient Tandem Solar Cells. *Advanced Materials* **2024,** *36* (9), 2307701.
12. Hang, P.; Kan, C.; Li, B.; Yao, Y.; Hu, Z.; Zhang, Y.; Xie, J.; Wang, Y.; Yang, D.; Yu, X., Highly Efficient and Stable Wide-Bandgap Perovskite Solar Cells via Strain Management. *Advanced Functional Materials* **2023,** *33* (11), 2214381.
13. Lin, Y.-H.; null, V.; Yang, F.; Cao, X.-L.; Dasgupta, A.; Oliver, R. D. J.; Ulatowski, A. M.; McCarthy, M. M.; Shen, X.; Yuan, Q.; Christoforo, M. G.; Yeung, F. S. Y.; Johnston, M. B.; Noel, N. K.; Herz, L. M.; Islam, M. S.; Snaith, H. J., Bandgap-universal passivation enables stable perovskite solar cells with low photovoltage loss. *Science* **2024,** *384* (6697), 767-775.
14. Qiao, L.; Ye, T.; Wang, T.; Kong, W.; Sun, R.; Zhang, L.; Wang, P.; Ge, Z.; Peng, Y.; Zhang, X.; Xu, M.; Yan, X.; Yang, J.; Zhang, X.; Zeng, F.; Han, L.; Yang, X., Freezing Halide Segregation Under Intense Light for Photostable Perovskite/Silicon Tandem Solar Cells. *Advanced Energy Materials* **2024,** *14* (7), 2302983.
15. Yan, N.; Gao, Y.; Yang, J.; Fang, Z.; Feng, J.; Wu, X.; Chen, T.; Liu, S., Wide-Bandgap Perovskite Solar Cell Using a Fluoride-Assisted Surface Gradient Passivation Strategy. *Angewandte Chemie International Edition* **2023,** *62* (11), e202216668.
16. Li, Z.; Sun, X.; Zheng, X.; Li, B.; Gao, D.; Zhang, S.; Wu, X.; Li, S.; Gong, J.; Luther, J. M.; Li, Z. a.; Zhu, Z., Stabilized hole-selective layer for high-performance inverted p-i-n perovskite solar cells. *Science* **2023,** *382* (6668), 284-289.
17. Ji, S. G.; Park, I. J.; Chang, H.; Park, J. H.; Hong, G. P.; Choi, B. K.; Jang, J. H.; Choi, Y. J.; Lim, H. W.; Ahn, Y. J.; Park, S. J.; Nam, K. T.; Hyeon, T.; Park, J.; Kim, D. H.; Kim, J. Y., Stable pure-iodide wide-band-gap perovskites for efficient Si tandem cells via kinetically controlled phase evolution. *Joule* **2022,** *6* (10), 2390-2405.
18. Tan, S.; Tan, C.; Cui, Y.; Yu, B.; Li, Y.; Wu, H.; Shi, J.; Luo, Y.; Li, D.; Meng, Q., Constructing an Interfacial Gradient Heterostructure Enables Efficient CsPbI3 Perovskite Solar Cells and Printed Minimodules. *Advanced Materials* **2023,** *35* (28), 2301879.

19. Yang, G.; Ren, Z.; Liu, K.; Qin, M.; Deng, W.; Zhang, H.; Wang, H.; Liang, J.; Ye, F.; Liang, Q.; Yin, H.; Chen, Y.; Zhuang, Y.; Li, S.; Gao, B.; Wang, J.; Shi, T.; Wang, X.; Lu, X.; Wu, H.; Hou, J.; Lei, D.; So, S. K.; Yang, Y.; Fang, G.; Li, G., Stable and low-photovoltage-loss perovskite solar cells by multifunctional passivation. *Nature Photonics* **2021,** *15* (9), 681-689.
20. Zhao, Y.; Wang, C.; Ma, T.; Zhou, L.; Wu, Z.; Wang, H.; Chen, C.; Yu, Z.; Sun, W.; Wang, A.; Huang, H.; Zou, B.; Zhao, D.; Li, X., Reduced 0.418 V VOC-deficit of 1.73 eV wide-bandgap perovskite solar cells assisted by dual chlorides for efficient all-perovskite tandems. *Energy & Environmental Science* **2023,** *16* (5), 2080-2089.
21. Jiang, Q.; Tong, J.; Scheidt, R. A.; Wang, X.; Louks, A. E.; Xian, Y.; Tirawat, R.; Palmstrom, A. F.; Hautzinger, M. P.; Harvey, S. P.; Johnston, S.; Schelhas, L. T.; Larson, B. W.; Warren, E. L.; Beard, M. C.; Berry, J. J.; Yan, Y.; Zhu, K., Compositional texture engineering for highly stable wide-bandgap perovskite solar cells. *Science* **2022,** *378* (6626), 1295-1300.
22. Chen, X.; Jia, Z.; Chen, Z.; Jiang, T.; Bai, L.; Tao, F.; Chen, J.; Chen, X.; Liu, T.; Xu, X.; Yang, C.; Shen, W.; Sha, W. E. I.; Zhu, H.; Yang, Y., Efficient and Reproducible Monolithic Perovskite/Organic Tandem Solar Cells with Low-Loss Interconnecting Layers. *Joule* **2020,** *4* (7), 1594-1606.
23. He, R.; Wang, W.; Yi, Z.; Lang, F.; Chen, C.; Luo, J.; Zhu, J.; Thiesbrummel, J.; Shah, S.; Wei, K.; Luo, Y.; Wang, C.; Lai, H.; Huang, H.; Zhou, J.; Zou, B.; Yin, X.; Ren, S.; Hao, X.; Wu, L.; Zhang, J.; Zhang, J.; Stolterfoht, M.; Fu, F.; Tang, W.; Zhao, D., Improving interface quality for 1-cm2 all-perovskite tandem solar cells. *Nature* **2023,** *618* (7963), 80-86.
24. Yi, Z.; Wang, W.; He, R.; Zhu, J.; Jiao, W.; Luo, Y.; Xu, Y.; Wang, Y.; Zeng, Z.; Wei, K.; Zhang, J.; Tsang, S.-W.; Chen, C.; Tang, W.; Zhao, D., Achieving a high open-circuit voltage of 1.339 V in 1.77 eV wide-bandgap perovskite solar cells via self-assembled monolayers. *Energy & Environmental Science* **2024,** *17* (1), 202-209.
25. Cui, H.; Huang, L.; Zhou, S.; Wang, C.; Hu, X.; Guan, H.; Wang, S.; Shao, W.; Pu, D.; Dong, K.; Zhou, J.; Jia, P.; Wang, W.; Tao, C.; Ke, W.; Fang, G., Lead halide coordination competition at buried interfaces for low VOC-deficits in wide-bandgap perovskite solar cells. *Energy & Environmental Science* **2023,** *16* (12), 5992-6002.
26. Qin, S.; Lu, C.; Jia, Z.; Wang, Y.; Li, S.; Lai, W.; Shi, P.; Wang, R.; Zhu, C.; Du, J.; Zhang, J.; Meng, L.; Li, Y., Constructing Monolithic Perovskite/Organic Tandem Solar Cell with Efficiency of 22.0% via Reduced Open-Circuit Voltage Loss and Broadened Absorption Spectra. *Advanced Materials* **2022,** *34* (11), 2108829.
27. Chen, W.; Zhu, Y.; Xiu, J.; Chen, G.; Liang, H.; Liu, S.; Xue, H.; Birgersson, E.; Ho, J. W.; Qin, X.; Lin, J.; Ma, R.; Liu, T.; He, Y.; Ng, A. M.-C.; Guo, X.; He, Z.; Yan, H.; Djurišić, A. B.; Hou, Y., Monolithic perovskite/organic tandem solar cells with 23.6% efficiency enabled by reduced voltage losses and optimized interconnecting layer. *Nature Energy* **2022,** *7* (3), 229-237.
28. Chen, H.; Maxwell, A.; Li, C.; Teale, S.; Chen, B.; Zhu, T.; Ugur, E.; Harrison, G.; Grater, L.; Wang, J.; Wang, Z.; Zeng, L.; Park, S. M.; Chen, L.; Serles, P.; Awni, R. A.; Subedi, B.; Zheng, X.; Xiao, C.; Podraza, N. J.; Filleter, T.; Liu, C.; Yang, Y.; Luther, J. M.; De Wolf, S.; Kanatzidis, M. G.; Yan, Y.; Sargent, E. H., Regulating surface potential maximizes voltage in all-perovskite tandems. *Nature* **2023,** *613* (7945), 676-681.
29. Chen, M.; Li, Y.; Zeng, Z.; Liu, M.; Du, T.; Huang, X.; Bi, L.; Wang, J.; Jiang, W.; An, Y.; Tsang, S.-W.; Yin, J.; Wu, S.; Jen, A. K. Y., Regulating the crystallization of mixed-halide perovskites by cation alloying for perovskite–organic tandem solar cells. *Energy & Environmental Science* **2024,** *17* (24),

9580-9589.
30. Wen, J.; Zhao, Y.; Liu, Z.; Gao, H.; Lin, R.; Wan, S.; Ji, C.; Xiao, K.; Gao, Y.; Tian, Y.; Xie, J.; Brabec, C. J.; Tan, H., Steric Engineering Enables Efficient and Photostable Wide-Bandgap Perovskites for All-Perovskite Tandem Solar Cells. *Advanced Materials* **2022,** *34* (26), 2110356.
31. Yang, F.; Tockhorn, P.; Musiienko, A.; Lang, F.; Menzel, D.; Macqueen, R.; Köhnen, E.; Xu, K.; Mariotti, S.; Mantione, D.; Merten, L.; Hinderhofer, A.; Li, B.; Wargulski, D. R.; Harvey, S. P.; Zhang, J.; Scheler, F.; Berwig, S.; Roß, M.; Thiesbrummel, J.; Al-Ashouri, A.; Brinkmann, K. O.; Riedl, T.; Schreiber, F.; Abou-Ras, D.; Snaith, H.; Neher, D.; Korte, L.; Stolterfoht, M.; Albrecht, S., Minimizing Interfacial Recombination in 1.8 eV Triple-Halide Perovskites for 27.5% Efficient All-Perovskite Tandems. *Advanced Materials* **2024,** *36* (6), 2307743.
32. Wu, S.; Yan, Y.; Yin, J.; Jiang, K.; Li, F.; Zeng, Z.; Tsang, S.-W.; Jen, A. K. Y., Redox mediator-stabilized wide-bandgap perovskites for monolithic perovskite-organic tandem solar cells. *Nature Energy* **2024,** *9* (4), 411-421.
33. Brinkmann, K. O.; Becker, T.; Zimmermann, F.; Kreusel, C.; Gahlmann, T.; Theisen, M.; Haeger, T.; Olthof, S.; Tückmantel, C.; Günster, M.; Maschwitz, T.; Göbelsmann, F.; Koch, C.; Hertel, D.; Caprioglio, P.; Peña-Camargo, F.; Perdigón-Toro, L.; Al-Ashouri, A.; Merten, L.; Hinderhofer, A.; Gomell, L.; Zhang, S.; Schreiber, F.; Albrecht, S.; Meerholz, K.; Neher, D.; Stolterfoht, M.; Riedl, T., Perovskite–organic tandem solar cells with indium oxide interconnect. *Nature* **2022,** *604* (7905), 280-286.
34. An, Y.; Zhang, N.; Zeng, Z.; Cai, Y.; Jiang, W.; Qi, F.; Ke, L.; Lin, F. R.; Tsang, S.-W.; Shi, T.; Jen, A. K. Y.; Yip, H.-L., Optimizing Crystallization in Wide-Bandgap Mixed Halide Perovskites for High-Efficiency Solar Cells. *Advanced Materials* **2024,** *36* (17), 2306568.
35. Wang, X.; Zhang, D.; Liu, B.; Wu, X.; Jiang, X.; Zhang, S.; Wang, Y.; Gao, D.; Wang, L.; Wang, H.; Huang, Z.; Xie, X.; Chen, T.; Xiao, Z.; He, Q.; Xiao, S.; Zhu, Z.; Yang, S., Highly Efficient Perovskite/Organic Tandem Solar Cells Enabled by Mixed-Cation Surface Modulation. *Advanced Materials* **2023,** *35* (49), 2305946.
36. Xiang, W.; Wang, Z.; Kubicki, D. J.; Wang, X.; Tress, W.; Luo, J.; Zhang, J.; Hofstetter, A.; Zhang, L.; Emsley, L.; Grätzel, M.; Hagfeldt, A., Ba-induced phase segregation and band gap reduction in mixed-halide inorganic perovskite solar cells. *Nature Communications* **2019,** *10* (1), 4686.
37. Guo, Z.; Zhao, S.; Shibayama, N.; Kumar Jena, A.; Takei, I.; Miyasaka, T., A Universal Method of Perovskite Surface Passivation for CsPbX3 Solar Cells with VOC over 90% of the S-Q limit. *Advanced Functional Materials* **2022,** *32* (43), 2207554.
38. Fu, S.; Li, X.; Wan, L.; Zhang, W.; Song, W.; Fang, J., Effective Surface Treatment for High-Performance Inverted CsPbI2Br Perovskite Solar Cells with Efficiency of 15.92%. *Nano-Micro Letters* **2020,** *12* (1), 170.
39. Guo, X.; Jia, Z.; Liu, S.; Guo, R.; Jiang, F.; Shi, Y.; Dong, Z.; Luo, R.; Wang, Y.-D.; Shi, Z.; Li, J.; Chen, J.; Lee, L. K.; Müller-Buschbaum, P.; Ginger, D. S.; Paterson, D. J.; Hou, Y., Stabilizing efficient wide-bandgap perovskite in perovskite-organic tandem solar cells. *Joule* **2024,** *8* (9), 2554-2569.
40. Fang, Z.; Meng, X.; Zuo, C.; Li, D.; Xiao, Z.; Yi, C.; Wang, M.; Jin, Z.; Yang, S.; Ding, L., Interface engineering gifts CsPbI2.25Br0.75 solar cells high performance. *Science Bulletin* **2019,** *64* (23), 1743-1746.
41. Li, Z.; Kim, T. H.; Han, S. Y.; Yun, Y.-J.; Jeong, S.; Jo, B.; Ok, S. A.; Yim, W.; Lee, S. H.; Kim, K.; Moon, S.; Park, J.-Y.; Ahn, T. K.; Shin, H.; Lee, J.; Park, H. J., Wide-Bandgap Perovskite/Gallium Arsenide Tandem Solar Cells. *Advanced Energy Materials* **2020,** *10* (6), 1903085.

42. Nguyen, T. T.; Kim, J.; Kim, Y. S.; Nguyen, B. P.; Jo, W., Wide-bandgap perovskites for multijunction solar cells: improvement of crystalline quality of Cs0.1FA0.9PbI1.4Br1.6 by using lead thiocyanate. *Journal of Materials Chemistry A* **2023,** *11* (19), 10254-10266.
43. Sun, H.; Zhang, J.; Gan, X.; Yu, L.; Yuan, H.; Shang, M.; Lu, C.; Hou, D.; Hu, Z.; Zhu, Y.; Han, L., Pb-Reduced CsPb0.9Zn0.1I2Br Thin Films for Efficient Perovskite Solar Cells. *Advanced Energy Materials* **2019,** *9* (25), 1900896.
44. Yao, Q.; Xie, Y.-M.; Zhou, Y.; Xue, Q.; Xu, X.; Gao, Y.; Niu, T.; Chu, L.; Zhou, Z.; Lin, F. R.; Jen, A. K. Y.; Shi, T.; Yip, H.-L.; Cao, Y., Dual Sub-Cells Modification Enables High-Efficiency n–i–p Type Monolithic Perovskite/Organic Tandem Solar Cells. *Advanced Functional Materials* **2023,** *33* (8), 2212599.
45. Jiang, X.; Qin, S.; Meng, L.; He, G.; Zhang, J.; Wang, Y.; Zhu, Y.; Zou, T.; Gong, Y.; Chen, Z.; Sun, G.; Liu, M.; Li, X.; Lang, F.; Li, Y., Isomeric diammonium passivation for perovskite–organic tandem solar cells. *Nature* **2024,** *635* (8040), 860-866.
46. Fan, Y.; Fang, J.; Chang, X.; Tang, M.-C.; Barrit, D.; Xu, Z.; Jiang, Z.; Wen, J.; Zhao, H.; Niu, T.; Smilgies, D.-M.; Jin, S.; Liu, Z.; Li, E. Q.; Amassian, A.; Liu, S.; Zhao, K., Scalable Ambient Fabrication of High-Performance CsPbI₂Br Solar Cells. *Joule* **2019,** *3* (10), 2485-2502.
47. Zhang, S.; Chen, W.; Wu, S.; Chen, R.; Liu, Z.; Huang, Y.; Yang, Z.; Zhu, H.; Li, J.; Han, L.; Chen, W., Hybrid Inorganic Electron-Transporting Layer Coupled with a Halogen-Resistant Electrode in CsPbI2Br-Based Perovskite Solar Cells to Achieve Robust Long-Term Stability. *ACS Applied Materials & Interfaces* **2019,** *11* (46), 43303-43311.
48. Gu, X.; Lai, X.; Zhang, Y.; Wang, T.; Tan, W. L.; McNeill, C. R.; Liu, Q.; Sonar, P.; He, F.; Li, W.; Shan, C.; Kyaw, A. K. K., Organic Solar Cell With Efficiency Over 20% and VOC Exceeding 2.1 V Enabled by Tandem With All-Inorganic Perovskite and Thermal Annealing-Free Process. *Advanced Science* **2022,** *9* (28), 2200445.
49. Wu, X.; Zhang, D.; Liu, B.; Wang, Y.; Wang, X.; Liu, Q.; Gao, D.; Wang, N.; Li, B.; Wang, L.; Yu, Z.; Li, X.; Xiao, S.; Li, N.; Stolterfoht, M.; Lin, Y.-H.; Yang, S.; Zeng, X. C.; Zhu, Z., Optimization of Charge Extraction and Interconnecting Layers for Highly Efficient Perovskite/Organic Tandem Solar Cells with High Fill Factor. *Advanced Materials* **2024,** *36* (49), 2410692.
50. Sun, S.-Q.; Xu, X.; Sun, Q.; Yao, Q.; Cai, Y.; Li, X.-Y.; Xu, Y.-L.; He, W.; Zhu, M.; Lv, X.; Lin, F. R.; Jen, A. K. Y.; Shi, T.; Yip, H.-L.; Fung, M.-K.; Xie, Y.-M., All-Inorganic Perovskite-Based Monolithic Perovskite/Organic Tandem Solar Cells with 23.21% Efficiency by Dual-Interface Engineering. *Advanced Energy Materials* **2023,** *13* (16), 2204347.
51. Wang, J.; Zeng, L.; Zhang, D.; Maxwell, A.; Chen, H.; Datta, K.; Caiazzo, A.; Remmerswaal, W. H. M.; Schipper, N. R. M.; Chen, Z.; Ho, K.; Dasgupta, A.; Kusch, G.; Ollearo, R.; Bellini, L.; Hu, S.; Wang, Z.; Li, C.; Teale, S.; Grater, L.; Chen, B.; Wienk, M. M.; Oliver, R. A.; Snaith, H. J.; Janssen, R. A. J.; Sargent, E. H., Halide homogenization for low energy loss in 2-eV-bandgap perovskites and increased efficiency in all-perovskite triple-junction solar cells. *Nature Energy* **2024,** *9* (1), 70-80.
52. Wang, Z.; Zeng, L.; Zhu, T.; Chen, H.; Chen, B.; Kubicki, D. J.; Balvanz, A.; Li, C.; Maxwell, A.; Ugur, E.; dos Reis, R.; Cheng, M.; Yang, G.; Subedi, B.; Luo, D.; Hu, J.; Wang, J.; Teale, S.; Mahesh, S.; Wang, S.; Hu, S.; Jung, E. D.; Wei, M.; Park, S. M.; Grater, L.; Aydin, E.; Song, Z.; Podraza, N. J.; Lu, Z.-H.; Huang, J.; Dravid, V. P.; De Wolf, S.; Yan, Y.; Grätzel, M.; Kanatzidis, M. G.; Sargent, E. H., Suppressed phase segregation for triple-junction perovskite solar cells. *Nature* **2023,** *618* (7963), 74-79.